Multiple bifurcations in atom optics

W. K. Hensinger,[1] B. Upcroft,[1] C. A. Holmes,[2] N. R. Heckenberg,[1] G. J. Milburn,[3] and H. Rubinsztein-Dunlop[1]
[1]*Centre for Laser Science, Department of Physics, The University of Queensland, Brisbane, Queensland 4072, Australia*
[2]*Department of Mathematics, The University of Queensland, Brisbane, Queensland 4072, Australia*
[3]*Centre for Quantum Computer Technology, Department of Physics, The University of Queensland, Brisbane, Queensland 4072, Australia*
(Received 7 July 2001; published 16 November 2001)

We report the observation of multiple bifurcations in a nonlinear Hamiltonian system: laser-cooled atoms in a standing wave with single-frequency intensity modulation. We provide clear evidence of the occurrence of bifurcations by analyzing the atomic momentum distributions.

DOI: 10.1103/PhysRevA.64.063408 PACS number(s): 42.50.Vk, 32.80.Pj, 05.45.Mt, 03.75.Be

I. INTRODUCTION

Laser-cooled atoms moving in far off-resonant optical-dipole potentials have provided a clean and versatile experimental context for the investigation of the quantum dynamics of nonlinear Hamiltonian systems. Previous work [1,3–7] has demonstrated the ability to achieve nondissipative dynamics in the quantum domain (dimensionless Planck's constant of the order of unity) with well-controlled time-dependent potentials. Sinusoidal potentials with a periodically modulated phase were used [1,2] to achieve quantum localization of the momentum. A detailed comparison was made of the classical phase-space structure and quantum dynamics with experiments, as a function of the driving strength, in the work of Robinson *et al.* [3]. Experiments to test the resonance overlap criteria where atoms were subjected to an amplitude-modulated standing wave for one modulation period [4] showed that the phase space changed from global stability to chaotic. This could be concluded from an analysis of the atomic momentum distribution. Subsequently a close approximation to the δ-kicked rotor was implemented by using an amplitude-modulated standing wave [5]. The atoms were subjected to a periodic sequence of short pulses of a standing wave, with the pulse width much shorter than the repetition period. Effectively this corresponds to broad-band amplitude modulation centered on the pulse frequency. In contrast, in this paper we consider cold atoms moving in a sinusoidal optical-dipole potential with amplitude modulation at a single frequency that corresponds to the classical driven pendulum, a textbook example for theoretical studies of nonlinear Hamiltonian systems. In earlier work we reported the observation and initial theoretical analysis of phase-space resonances in this system and pathways to study quantum chaos and dynamical tunneling [6,7].

In this paper we present an experimental and theoretical study of the classical phase-space structure, and its bifurcations, as a function of the scaled well depth κ of the intensity-modulated standing wave. In our experiments, we observed the bifurcation sequence as distinct peaks in the atomic momentum distribution that appear and disappear when one of the control parameters of the system is changed. We show that the observation of multiple bifurcations can be explained by classical Hamiltonian theory. For further discussion of bifurcation theory, see, for example, [8,9]. Bifurcations have been observed in other Hamiltonian systems such as the absorption spectra of atoms in electric and magnetic fields. Experimental measurements showed that the stable periodic electron-orbits bifurcated to new orbits of longer period [10,11].

The phase space of the driven pendulum is two dimensional, with position and momentum coordinates describing the motion of the atoms along the direction of the standing wave. When the standing wave is modulated a mixed phase-space results. In Fig. 1 we show Poincaré sections with the stroboscopic period equal to the modulation period. The two islands of stability left and right of the center result from phase-space resonances and correspond to atoms that oscillate in phase with the standing-wave modulation. The inner island corresponds to atoms that are approximately stationary at the bottom of the well. The sea of chaotic motion is bounded in momentum by the region of regular unbound motion that consists of atoms having enough kinetic energy to hop from one standing-wave well to the next. The period of a resonance determines how many periods of the modulation frequency it takes for the atoms to return to their original position in the phase space. For example, atoms in a period 2 resonance need two periods of the modulation frequency to return to their initial phase-space coordinate. The islands of regular motion near the region of unbound regular motion are librations: atoms that take multiples of one modulation period to hop from one well to another.

II. THE DRIVEN PENDULUM IN ATOM OPTICS AND ITS EXPERIMENTAL IMPLEMENTATION

To observe these phase-space resonances we carried out experiments using cold rubidium atoms that are positioned in a far detuned optical standing wave. Single-frequency modulation of the intensity of the standing wave leads to an effective Hamiltonian for the center-of-mass motion (by adiabatically eliminating the excited state) [6,12] given by

$$H=\frac{p_x^2}{2m}+\frac{\hbar\Omega_{\mathrm{eff}}}{4}(1-2\varepsilon\sin\omega t)\sin^2(kx), \qquad (1)$$

where the effective Rabi frequency is $\Omega_{\mathrm{eff}}=\Omega^2/\delta$, $\Omega=\Gamma\sqrt{I/I_{\mathrm{sat}}}$ is the resonant Rabi frequency, ε is the modula-

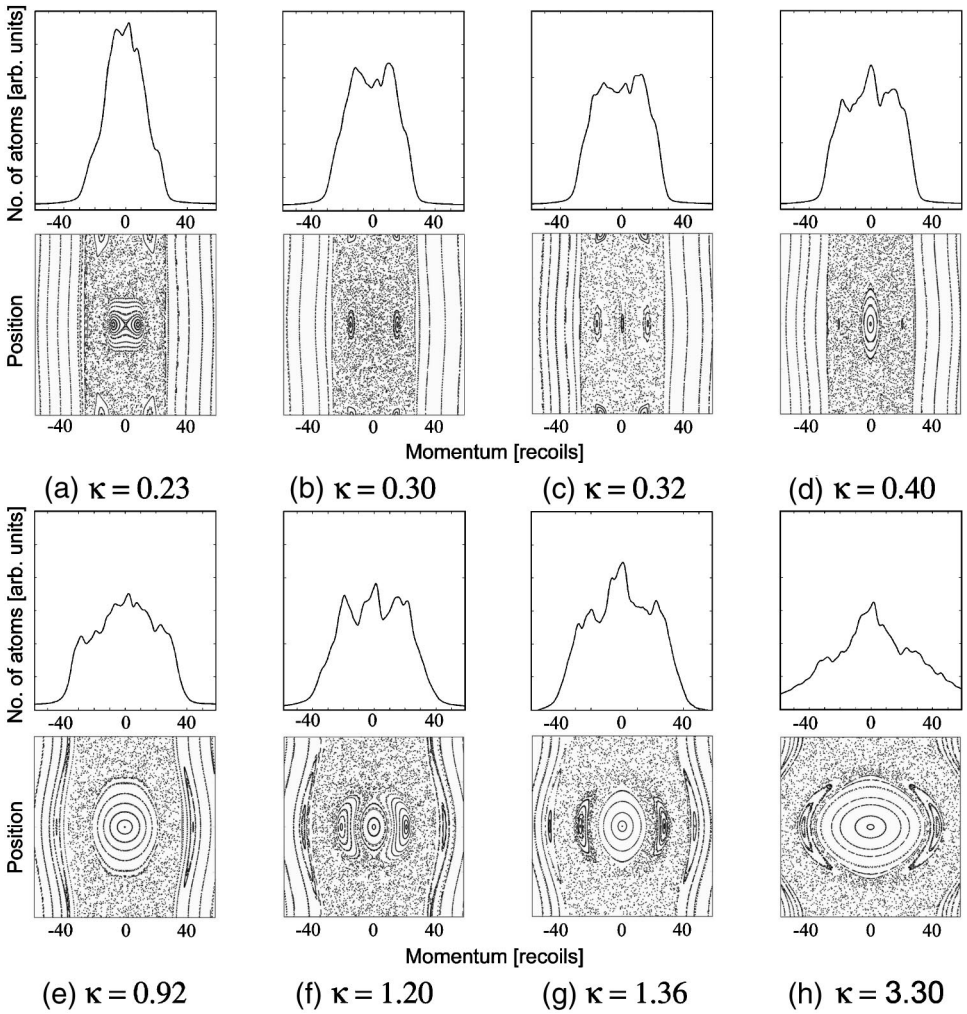

FIG. 1. Bifurcation sequence. The upper pictures are the experimentally measured momentum distributions. The corresponding classical Poincaré sections are shown below where the x axis is the momentum coordinate in recoils and the y axis is the position coordinate along the standing wave. The resonances appear as distinct peaks in the momentum distribution. When the scaled well depth κ is increased several bifurcations occur in this mixed phase space.

tion parameter, ω is the modulation angular frequency, Γ is the inverse spontaneous lifetime, δ is the detuning of the standing wave, t is the time, p_x the momentum component of the atom along the standing wave, and k is the wave number. Here I is the spatial mean of the intensity of the unmodulated standing wave (which is half of the peak intensity) so $\Omega = \Gamma \sqrt{I_{\text{peak}}/2I_{\text{sat}}}$ and $I_{\text{sat}} = hc\Gamma/\lambda^3$ is the saturation intensity. λ is the wavelength of the standing wave. Using scaled variables [5,6] the Hamiltonian is given by

$$\mathcal{H} = p^2/2 + 2\kappa(1 - 2\varepsilon \sin\tau)\sin^2(q/2), \tag{2}$$

where $\mathcal{H} = (4k^2/m\omega^2)H$, $q = 2kx$, and $p = (2k/m\omega)p_x$. The driving amplitude is given by

$$\kappa = \frac{\hbar k^2 \Omega_{\text{eff}}}{2\omega^2 m} \tag{3}$$

and $\tau = t\omega$ is the scaled time variable. A thorough theoretical derivation along with the relevant classical and quantum simulation methods can be found in Ref. [6].

Our experimental setup consists of a standard magneto-optic trap (MOT) for rubidium atoms. A titanium sapphire laser is used to produce an optical standing wave. The standing wave is modulated using an acousto-optic modulator. To load resonances experimentally we choose the starting phase of the modulation in such a way that the resonances are located on the position axis where they overlap with the initial atomic momentum distribution. To observe phase-space resonances we choose the endphase of the intensity modulation so that the resonances are located on the momentum axis having equal but oppositely directed nonzero momentum. After approximately 10 ms ballistic expansion time a picture of the atomic distribution is taken using a freezing molasses method. Resonances can be observed as distinct peaks in the atomic momentum distribution (atomic position distribution after ballistic expansion) resulting in experimental data as shown in Fig. 1. Details of the experimental setup may be found in Refs. [6,7].

To illustrate this bifurcation sequence we use the scaled well depth κ as the control parameter. The driving amplitude κ and the momentum coordinate p are scaled with modulation frequency ω. For the experiments we have presented here we have kept the modulation frequency constant at 300 kHz, so that experiments with different values of κ can be compared using real momentum coordinates. To change the value of κ we have adjusted the detuning δ of the modulated standing wave while we left the intensity I constant. The intensity measurement error was $+8\%$ -5% and it is a systematic error that is the same for all of our data. The error

in the detuning of the standing wave was smaller than 3% and it is a random error given by the accuracy of the wave meter we have used.

The modulation frequency used in our experiments corresponds to a scaled Planck's constant of 0.1. The scaled Planck's constant [6,7] is the ratio of Planck's constant to the typical action of a particle in our system.

III. THE BIFURCATION SEQUENCE

Figure 1 shows the bifurcation sequence in terms of the Poincaré sections along with the corresponding experimental momentum distributions. All the observed resonances bifurcate from the origin, where the oscillation frequency is $\sqrt{\kappa}$. Since a period-(n/m) resonance occurs when the period of the oscillation is n/m times the period of the driving, a period-(n/m) resonance bifurcates when $\kappa=(m^2/n^2)+O(\epsilon)$, where n and m are integers. Here the particular perturbation implies that only resonances with $n\geqslant 2$ and even, $m\geqslant 1$ occur. Those with $n=2$ can be easily seen in Poincaré sections in Fig. 1, appearing as two symmetrically placed resonance islands. They are also of particular interest experimentally as they can be easily identified in the experimental momentum distribution as two peaks, on either side of the center.

To obtain the dependence of the bifurcation on ϵ we use classical perturbation theory about the origin. We assume that the state variables (p,q) are of order $\sqrt{\epsilon}$. For κ close to resonance $(\kappa\approx m^2/n^2)$, we can use canonical perturbation theory to give us a fairly accurate picture of the emerging resonances. We expand κ as a series in ϵ about the resonance

$$\kappa=\kappa_0+\epsilon\kappa_1+\epsilon^2\kappa_2+\cdots, \tag{4}$$

where κ_0 is the value at resonance with $\kappa_0=\frac{1}{4}$, 1, and $\frac{9}{4}$ for the resonances that we see experimentally. Near the origin q is small and on the order $\sqrt{\epsilon}$ so that $[\sin(q/2)]^2$ may be approximated by the first-few terms in its Taylor series about zero.

Then to zeroth order in ϵ

$$H=H_0=\frac{p^2}{2}+\kappa_0\frac{q^2}{2}, \tag{5}$$

which has action-angle variables (I,θ) where

$$p=\kappa_0^{1/4}\sqrt{2I}\cos\theta,\quad q=\frac{\sqrt{2I}}{\kappa_0^{1/4}}\sin\theta. \tag{6}$$

Hence the Hamiltonian becomes

$$H(I,\theta,\tau)=\sqrt{\kappa_0}I+H_1(I,\theta,\tau)+H_2(I,\theta,\tau)+\cdots, \tag{7}$$

where H_m is $(m+1)$th order in ϵ. H_m has resonant oscillatory terms, $\cos(m\tau-n\theta)$ where n is even, implying mth-order resonances at the origin when $n\sqrt{\kappa_0}=m$.

To investigate the resonance at $\kappa_0=\frac{1}{4}$ we use two canonical transformations. The first is a near-identity transformation $I'=I+O(\epsilon)$, $\theta'=\theta+O(\epsilon)$ that removes all the oscillating terms, except those that are resonant. The transformed Hamiltonian is then

$$H=\sqrt{\kappa_0}I'-\frac{I'^2}{16}+\epsilon\frac{\sqrt{\kappa_0}}{2}I'\cos(\tau-2\theta')-\epsilon\frac{\kappa_1}{2\sqrt{\kappa_0}}I'+\cdots. \tag{8}$$

The second transformation consists of moving to a rotating frame $I'=J$, $\phi=\theta'-(\tau/2)$. In this rotating frame the Hamiltonian is

$$K=\epsilon\kappa_1 J-\frac{1}{16}J^2+\frac{\epsilon}{4}J\cos(2\phi)+\cdots. \tag{9}$$

If we now let $\bar{p}=\sqrt{J}\sin(\phi)$ and $\bar{q}=2\sqrt{J}\cos(\phi)$, the system of equations for $\bar{p}$ and $\bar{q}$ has stable fixed points on the (transformed) momentum axis that correspond to period-2 resonances of the original system. Since at a fixed point, ϕ is a constant so that $\theta=\tau/2+\text{const}$, the period of θ is twice the forcing period ($\phi=\tau-2\theta$ implies a period-2 resonance). Thus they rotate with half the modulation frequency. By including higher-order terms in the Hamiltonian we can show that these fixed points only exist for $\kappa>\frac{1}{4}(1-\epsilon+\epsilon^2-\epsilon^3)$, and that they destabilize the origin. They are just apparent in the Poincaré Map (a) in Fig. 1. As κ is increased the islands move apart and become separated by a sea of chaos as shown in (b). Then for $\kappa>\frac{1}{4}(1+\epsilon+\epsilon^2+\epsilon^3)$ two unstable fixed points bifurcate into the (transformed) position axis, stabilizing the origin once again. Between these two curves, which are shown in Fig. 2, the momentum distribution is clearly depressed in the center as shown in Fig. 1(b), whereas for $\kappa>\frac{1}{4}(1+\epsilon+\epsilon^2+\epsilon^3)$, at (c) the three distinct islands of regular motion appear clearly as three peaks in the momentum distribution. As κ increases further, the period-2 islands move out, breaking up as they do so and eventually become indistinguishable from the chaotic sea [Figs. 1(d) and 1(e)]. In Fig. 1 many of the Poincaré sections also show librational resonances. As they do not rotate they will not cross the position axis and therefore they are not loaded by the initial atomic momentum distribution in our current experimental setup. Thus they do not appear in the experimentally measured momentum distribution.

The resonance at $\kappa_0=1$ is of second order, meaning that it is only apparent once the first-order oscillatory terms have been removed via a near-identity transformation. This introduces further resonant terms of the form $\cos(2\tau-2\theta)$ giving rise to period-1 resonances as shown in Fig. 1(f) and 1(g). Once again to investigate them further two canonical transformations must be made. The second, as before, transforms to a rotating frame, but here $\phi=\theta'-\tau$. What follows is similar to the $\kappa=\frac{1}{4}$ case. Two similar bifurcations stabilizing and then destabilizing the origin take place for

$$\kappa=1+\frac{5\epsilon^2}{3}\quad\text{and}\quad\kappa=1-\frac{5\epsilon^2}{3}. \tag{10}$$

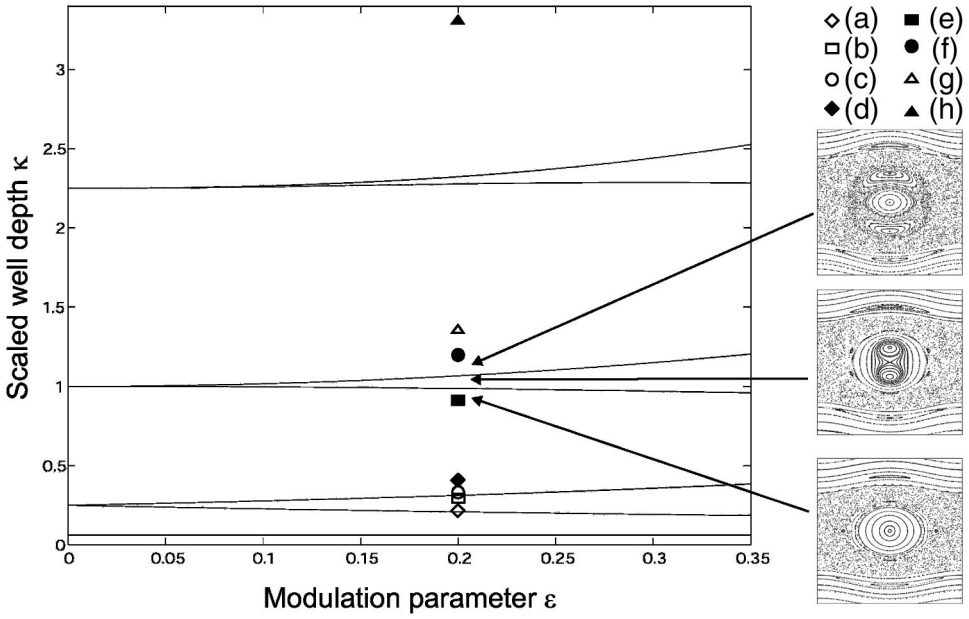

FIG. 2. The bifurcation diagram for the driven pendulum in atom optics. When the scaled well depth κ is changed the system undergoes multiple bifurcations. The values of κ where bifurcations occur depend on the modulation parameter ϵ. Three Poincaré sections are plotted. The arrows indicate to which part of the bifurcation diagram they correspond. The x axis in the Poincaré sections is the position coordinate and the y axis is the momentum coordinate. Symbols illustrating the corresponding parts of Fig. 1 are shown: ◇ as (a), □ (b), ○ (c), ◆ (d), ■ (e), ● (f), △ (g), and ▲ (h).

They are now of the order of ϵ^2 apart, which makes the individual bifurcations difficult to see experimentally. In Fig. 2, the bifurcation curves have been plotted in (ϵ,κ) space.

The pattern is repeated again for the third-order resonance at $\kappa=\frac{9}{4}$, due to the presence of $\cos(3\tau-2\theta)$ terms. The bifurcation curves are of the order of ϵ^3 apart and they are given by

$$\kappa=\frac{9}{4}+\frac{81\epsilon^2}{64}+\frac{81\epsilon^3}{256} \quad \text{and} \quad \kappa=\frac{9}{4}+\frac{81\epsilon^2}{64}-\frac{81\epsilon^3}{256} \tag{11}$$

($\phi=3\tau-2\theta$ implies a period-2/3 resonance). As one expects the momentum separation between regions of unbound regular motion becomes larger when the value of κ is increased. This is due to the wells becoming effectively deeper. Figure 2 represents the experimental regime where we were able to map the bifurcation sequence. The bifurcation curves shown, for $\kappa\approx 1/4$, 1, and 9/4, are of the order of ϵ^3. For a deeper understanding of the bifurcation diagram we have plotted three Poincaré sections for the $\kappa=1$ bifurcation. The arrows indicate that part of the bifurcation diagram that they represent. The symbols in Fig. 2 indicate the corresponding parts of Fig. 1.

The lower experimental limit of the scaled well depth κ for this sequence is determined by the momentum width of our initial atomic cloud. The kinetic temperature of our cloud was approximately 10 μK. If the initial momentum spread of the atomic cloud is much wider than the momentum width of the resonances, resonances cannot be resolved anymore in the experimentally measured position distribution. This is because the resonance features then become submerged in the chaotic background. Immediately after the loading phase when the atomic density inside the chaotic region is equal to the density inside the islands of regular motion (both equal to the initial atomic density), resonances do not constitute a feature in the atomic momentum distribution. However, after sufficient time, atoms in the chaotic region can spread over a larger volume (filling the entire chaotic region) that leads to a smaller atomic density in the chaotic region. This results in a significant atomic number signal-to-noise ratio between the regular region and the chaotic region in the atomic momentum distribution. For values of κ far below 0.2 our initial atomic momentum distribution even extends past the resonances, over the chaotic region and into the region of regular unbound motion. This problem could be overcome by preparing atoms with a lower kinetic temperature as that would imply a decrease in the momentum width. Alternatively one could increase the modulation frequency. The upper limit of κ is determined by the laser intensity and the detuning of the standing wave. When the detuning of the standing wave becomes too small, incoherent transitions need to be considered and the adiabatic elimination of the excited state in our theory breaks down. The dynamics can no longer be described by the Hamiltonian that is presented here. Furthermore spontaneous emission will act as a source of dissipation.

To perform an accurate mapping of the experimental results to the bifurcation sequence we measured the rotation frequency of the resonances. This measurement determines the period of the resonances. To conduct these measurements we vary the length of the standing-wave modulation (which is equivalent to a variation of the endphase of modulation) measured in cycles and record the resulting atomic momentum distribution. Figure 3 shows the rotation-frequency measurements for the resonances bifurcating at $\kappa=0.25$. We plot atomic momentum distributions and the length of the modulation in cycles is given for each momentum distribution. Resonances can be observed clearly when they are located on the momentum axis when the standing wave is turned off and will disappear when located on the position axis at that time. At 7.5 modulation period one can see two distinct resonances. These have completely disappeared after eight modulation period (cycles). The resonances can again be seen as distinct peaks in the momentum distribution after 8.5

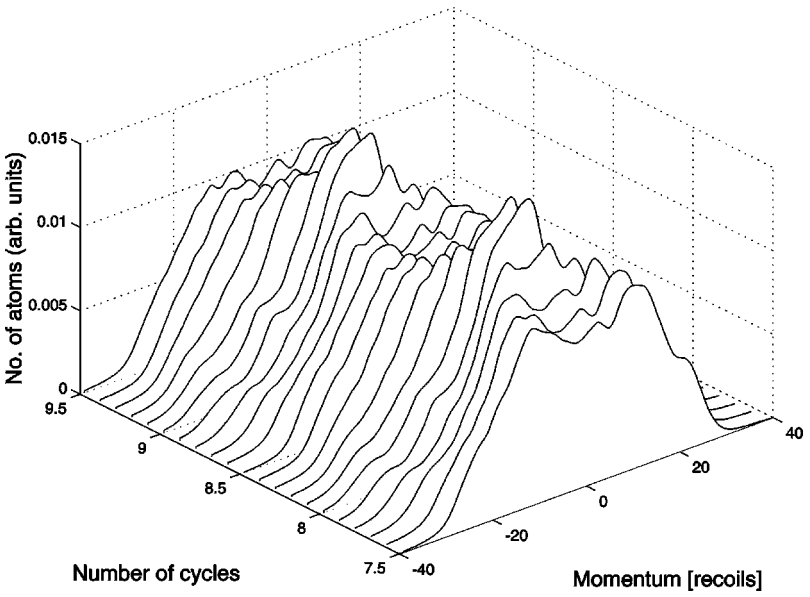

FIG. 3. Verification of the value of the period for the resonances at the $\kappa=0.25$ bifurcation. Atomic momentum distributions are shown for different modulation lengths measured in cycles. One can see that resonances return to their initial phase-space position after two periods of the standing-wave modulation.

periods of the standing-wave modulation. Therefore it follows that the resonances needed one modulation period to rotate by 180° in phase space. After two modulation periods the resonances appear again at their initial position. Hence, they are period-2 resonances.

Figure 4 shows the rotation frequency measurements for the resonances bifurcating at $\kappa\approx1$, which exhibits different features compared to Fig. 3. This allows us to distinguish between different bifurcation regimes. After 7.2 cycles one can see two distinct resonances and the center island of stability. A quarter period later, the resonances have rotated on the position axis and therefore no longer visible. Another quarter period later the resonances have rotated by 180° and are now located on the momentum axis. Note that the resonances have become wider and that their intensity has decreased as compared to the distribution at 7.2 periods of the standing-wave modulation. To understand this phenomenon one needs to consider the corresponding Poincaré sections as illustrated in Fig. 5. The left-hand side shows the phase space after 7.7 cycles, while the phase space after 7.2 cycles is shown on the right-hand side. Phase-space volume is preserved in Hamiltonian systems. However, the shape of the resonances has changed significantly. The momentum width of the resonance after 7.7 periods is larger compared to the one at 7.2 cycles. This results in the experimentally observed broadening of the resonances. From the discussion above it follows that these resonances need one modulation period to return to their initial position at $\kappa\approx1$ making them period-1 resonances.

We have also measured the rotational frequency for the period-2/3 resonances shown in Fig. 1(h). We were able to successfully confirm their period.

Figure 6 compares our experimental results with predictions from quantum trajectory simulations [6] and the classical description. We have measured the momentum of the center of the peak in the atomic momentum distributions

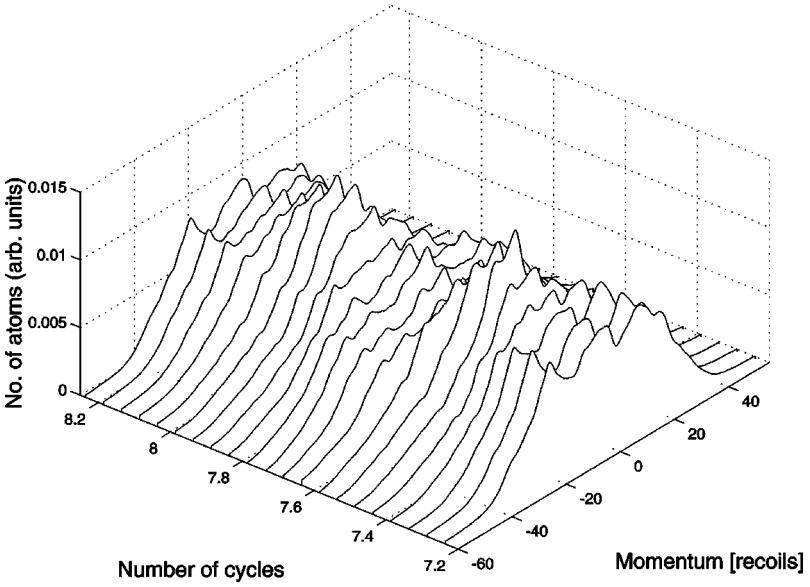

FIG. 4. Verification of the value of the period for the resonances at the $\kappa=1$ bifurcation. Atomic momentum distributions are shown for different modulation lengths measured in cycles. One can see that resonances return to their initial phase-space position after 1 period of the standing-wave modulation. When the resonances have rotated by 180° (7.7 cycles) with respect to their initial phase-space position (7.2 cycles) they have become wider compared to their initial width at 7.2 cycles.

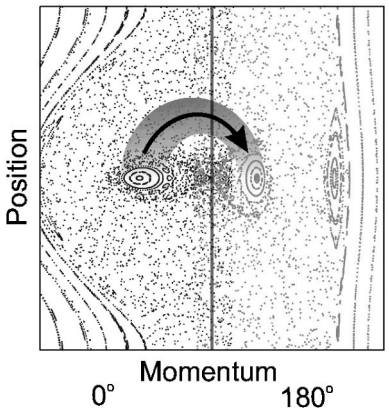

FIG. 5. A Poincaré section is shown for $\kappa=1.2$. While the left-hand side corresponds to 7.7 cycles, the right-hand side shows the corresponding phase space after a 180° rotation at 7.2 cycles. One can see that the momentum width of the resonances has significantly decreased.

both for the experimental data and the quantum simulations. The error bars for the experimental data result from the readout uncertainty due to asymmetries in the experimentally measured momentum distribution. These asymmetries are most likely due to nonuniformities in the initial spatial distribution of the MOT. Other possible error sources include an imperfectly zeroed magnetic field in the interaction region. The momenta of resonances in the quantum simulation exhibit some readout uncertainty because the peaks in the momentum distribution do not necessarily have a symmetric Gaussian shape. This readout uncertainty is reflected in the error bars for the quantum simulations.

We compare these results with the momentum of the resonances when they are located on the momentum axis, as calculated from numerical solutions of the equations describing the classical system and from classical perturbation theory. To zeroth order in ε, the momentum p of the period-(n/m) resonances is found by setting the nonlinear frequency $\omega(H)$ of the unperturbed system equal to m/n so that the momentum is given by

$$\omega(p^2/2)=\frac{m}{n}. \tag{12}$$

Here $\omega(H)$ is given by

$$\omega(H)=\frac{\pi\sqrt{\kappa}}{2F\left(\pi/2,\sqrt{\frac{H}{2\kappa}}\right)}, \tag{13}$$

where $F(\pi/2,\kappa)$ is the complete elliptic integral of the first kind. Canonical perturbation theory, here performed to order ε^2 and including the first three Fourier coefficients of the perturbation can be used to refine the result. As can be seen in Fig. 6 there is satisfactory agreement between the experimental results and the quantum simulations. The results taken from the Poincaré sections (numerical solution of Hamilton's equations) and the analytical classical results from perturbation theory are in good agreement. However, the classical predictions show a larger resonance momentum than the quantum simulations and the findings of our experiment. While the classical theory predicts the momentum of the fixed point (when positioned on the momentum axis), the quantum simulations directly predict the full momentum distribution as expected from the experiment. Part of the above discrepancy could result from the fact that the fixed points are positioned asymmetrically towards the faster side of the region of regular motion that in turn gives rise to the peak in the experimentally measured momentum distribution. However, if one assumes the mean of maximum and minimum momenta occupied by the region of regular motion (when positioned on the momentum axis) as a classical momentum approximation for the experimentally observed momentum peak, the classical resonance momenta are still significantly faster than the experimentally measured values. These results suggest a possible explanation in terms of the theory of quantum slow motion [13], but more rigorous and detailed investigation will be needed to confirm this.

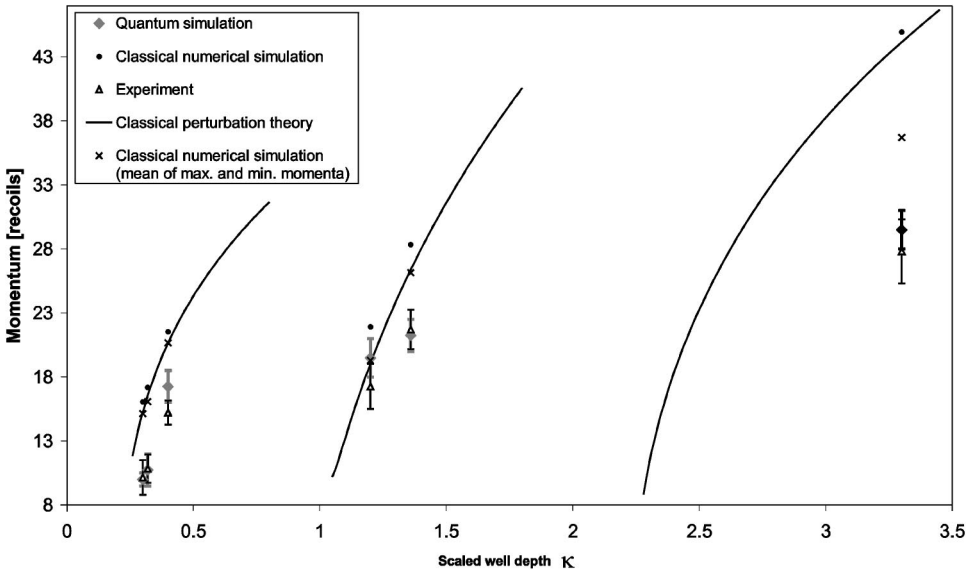

FIG. 6. Momenta of resonances in different bifurcation regimes. The momentum of different resonances is plotted as a function of the scaled well depth κ. These are compared with predictions from the quantum simulation, momentum of the fixed point in the Poincaré section (classical numerical simulation) when positioned on the momentum axis and results from classical perturbation theory. Furthermore we plot the mean of minimum and maximum momentum of the island of regular motion when positioned on the momentum axis obtained from the classical numerical simulation.

IV. CONCLUSION

For the first time we have been able to map a multiple bifurcation sequence in atom optics and explain their occurrence using classical perturbation theory for the relevant nonlinear Hamiltonian. Our experimental results are in good agreement with the theoretical predictions of classical perturbation theory highlighting the dynamics of cold atoms as a model system for truly nonlinear Hamiltonian dynamics. We have also succeeded in confirming the mapping of the atomic momentum distributions to the bifurcation diagram by measuring the rotation frequency of the resonant islands from which the distinct peaks in the atomic momentum distribution result. With the appropriate experimental conditions it is possible to extend the bifurcation sequence that was presented in this paper. With our current experimental setup we could extend it at the higher end by decreasing the modulation frequency and at the lower end by increasing the modulation frequency. By decreasing temperature and increasing laser intensity the range could also be substantially extended. The experimental system that was described here can be described by a truly two-dimensional phase space spanned by position and momentum along the standing wave making it an ideal testbed for experimental studies of nonlinear dynamics. When the scaled Planck's constant of the system becomes sufficiently large, one can use the dynamics of the driven pendulum in atom optics to study quantum tunneling phenomena [14], decoherence in nonlinear systems, and quantum chaos [7,12].

ACKNOWLEDGMENT

This work was supported by the Australian Research Council.

[1] F.L. Moore, J.C. Robinson, C.F. Bharucha, Bala Sundaram, and M.G. Raizen, Phys. Rev. Lett. **75**, 4598 (1995).
[2] R. Graham, M. Schlautmann, and P. Zoller, Phys. Rev. A **45**, R19 (1992).
[3] J.C. Robinson, C. Bharucha, F.L. Moore, R. Jahnke, G.A. Georgakis, Q. Niu, M.G. Raizen, and Bala Sundaram, Phys. Rev. Lett. **74**, 3963 (1995).
[4] J.C. Robinson, C.F. Bharucha, K.W. Madison, F.L. Moore, Bala Sundaram, S.R. Wilkinson, and M.G. Raizen, Phys. Rev. Lett. **76**, 3304 (1996).
[5] F.L. Moore, J.C. Robinson, C.F. Bharucha, Bala Sundaram, and M.G. Raizen, Phys. Rev. Lett. **75**, 4598 (1995).
[6] W.K. Hensinger, A.G. Truscott, B. Upcroft, M. Hug, H.M. Wiseman, N.R. Heckenberg, and H. Rubinsztein-Dunlop, Phys. Rev. A **64**, 033407 (2001).
[7] W.K. Hensinger, A.G. Truscott, B. Upcroft, N.R. Heckenberg, and H. Rubinsztein-Dunlop, J. Opt. B Quantum Semiclassical Opt. **2**, 659 (2000).
[8] A. J. Lichtenberg and M. A. Liebermann, *Regular Stochastic Motion*, Applied Mathematical Sciences Vol. 38 (Springer-Verlag, New York, 1988).
[9] M.A.M de Aguiar, C.P. Malta, M. Baranger, and K.T.R. Davises, Ann. Phys. (Paris) **180**, 167 (1987).
[10] J.-M. Mao, K.A. Rapelje, S.J. Blodgett-Ford, J.B. Delos, A. König, and H. Rinneberg, Phys. Rev. A **48**, 2117 (1993).
[11] J. Main, G. Wiebusch, K. Welge, J. Shaw, and J.B. Delos, Phys. Rev. A **49**, 847 (1994).
[12] S. Dyrting, G.J. Milburn, and C.A. Holmes, Phys. Rev. E **48**, 969 (1993).
[13] M. Hug and G.J. Milburn, Phys. Rev. A **63**, 023413 (2001).
[14] W.K. Hensinger, H. Häffner, A. Browaeys, N.R. Heckenberg, K. Helmerson, C. McKenzie, G.J. Milburn, W.D. Phillips, S.L. Rolston, H. Rubinsztein-Dunlop, and B. Upcroft, Nature (London) **412**, 52 (2001).